

17 **Abstract**

18 Carbon (C) saturation theory suggests that soils have a limited capacity to stabilize organic C and
19 that this capacity may be regulated by intrinsic soil properties such as clay concentration and
20 mineralogy. While C saturation theory has advanced our ability to predict soil C stabilization,
21 few biogeochemical ecosystem models have incorporated C saturation mechanisms. In
22 biogeochemical models, C and nitrogen (N) cycling are tightly coupled, with C decomposition
23 and respiration driving N mineralization. Thus, changing model structures from non-saturation
24 to C saturation dynamics can change simulated N dynamics. In this study, we used C saturation
25 models from the literature and of our own design to compare how different methods of modeling
26 C saturation affected simulated N mineralization dynamics. Specifically, we tested (i) how
27 modeling C saturation by regulating either the transfer efficiency (ϵ , g C retained g⁻¹ C respired)
28 or transfer rate (k) of C to stabilized pools affected N mineralization dynamics; (ii) how inclusion
29 of an explicit microbial pool through which C and N must pass affected N mineralization
30 dynamics; and (iii) whether using ϵ to implement C saturation in a model results in soil texture
31 controls on N mineralization that are similar to those currently included in widely used non-
32 saturating C and N models. Models were parameterized so that they rendered the same C
33 balance. We found that when C saturation is modeled using ϵ , the critical C:N ratio for N
34 mineralization from decomposing plant residues (r_{cr}) increases as C saturation of a soil
35 increases. When C saturation is modeled using k , however, r_{cr} is not affected by the C saturation
36 of a soil. Inclusion of an explicit microbial pool in the model structure was necessary to capture
37 short term N immobilization-mineralization turnover dynamics during decomposition of low N
38 residues. Finally, modelling C saturation by regulating ϵ led to similar soil texture controls on N
39 mineralization as a widely used non-saturating model, suggesting that C saturation may be a

40 fundamental mechanism that can explain N mineralization patterns across soil texture
41 gradients. These findings indicate that a coupled C and N model that includes saturation can (1)
42 represent short-term N-mineralization by including a microbial pool and (2) express the effects
43 of texture on N-turnover as an emergent property.

44 **1. Introduction**

45 Over the last two decades, the development of carbon (C) saturation theory has
46 fundamentally changed our understanding of C storage in soils and new biogeochemical models
47 have been developed to include C saturation dynamics (Hassink and Whitmore, 1997; Kemanian
48 et al., 2005; Stewart et al., 2007; Kemanian et al., 2011). In biogeochemical models that couple
49 C and nitrogen (N) cycles, C fluxes drive N mineralization (reviewed by Manzoni and Porporato,
50 2009). Thus, altering the structure of a C model to accommodate saturation dynamics is likely to
51 affect the coupled N cycle. Yet, few attempts have been made to understand how C saturation
52 affects N cycling (e.g. Castellano et al., 2012). In particular and to our knowledge, no study has
53 addressed how the C saturation models proposed in the literature affect simulated N
54 mineralization dynamics.

55 Carbon saturation theory suggests that soils have a limited capacity to stabilize organic C
56 and that this capacity may be regulated by intrinsic soil properties such as clay concentration and
57 mineralogy (Hassink, 1997; Six et al., 2002). Clay mineral surfaces stabilize and protect organic
58 C through mineral organic complexes, leading to reduced C decomposition rates (Baldock and
59 Skjemstad, 2000). As mineral surfaces in a soil become saturated with C, C decomposition rates
60 increase, and the rate of soil organic C storage per unit of C input declines. This phenomenon
61 results in an asymptotic response of soil organic C stocks to increasing C inputs (Stewart et al.,
62 2007; Gulde et al., 2008; Heitkamp et al., 2012). Six et al. (2002) proposed a conceptual model
63 of C protection based on measurable pools of organic C, including silt and clay associated C
64 pools and particulate organic matter C pools. Several studies have indicated that the silt and clay
65 associated C pools exhibit a saturating C storage response to increasing C inputs, while
66 particulate organic matter increases linearly with C inputs (Gulde et al., 2008; Stewart et al.,

2008; Stewart et al., 2012). Given these findings, a new generation of ecosystem models which can simulate physicochemical stabilization of soil organic matter by mineral surfaces, among other processes, are needed to incorporate recent advances in our understanding of C cycling (Schmidt et al., 2011).

Despite the strong evidence for C saturation, the majority of ecosystem scale biogeochemical models that couple C and N cycles use linear C models with no saturation (reviewed by Manzoni and Porporato, 2009). Rothamsted C (Jenkinson, 1990) and Century (Parton et al., 1987) are two widely used non-saturating C models. In these models, C decomposition occurs with first-order kinetics and steady-state C levels will increase linearly as C inputs increase. In C saturation models, however, steady-state C levels will approach an asymptotic limit as C inputs increase. Both non-saturation and saturation C models couple N mineralization and immobilization (N_{m-imm}) to C decomposition (C_{dec}) through the C:N ratio (r) of any given pair of decomposing (r_{dec}) and receiving (r_{rec}) pools and the C transfer efficiency (ϵ , g C g⁻¹ C) between pools (i.e. the proportion of decomposed C that is transferred to a receiving pool as organic C as opposed to being respired as CO₂, which is sometimes termed microbial growth efficiency). This coupling is represented as:

$$N_{m-imm} = C_{dec} \left(\frac{1}{r_{dec}} - \frac{\epsilon}{r_{rec}} \right) \quad (1)$$

The coupling of C and N described by Eq. (1) expresses a relationship between C decomposition, C respiration, and N mineralization that will be affected by the structure of a C saturation model. For instance, one way to implement C saturation dynamics is by regulating ϵ as a function of the C saturation ratio (the ratio of the actual C to that of a putative maximum C level of the saturating pool, C_s/C_x) (Stewart et al., 2007; Kemanian et al., 2011) (Fig. 1a).

89 Alternatively, the transfer rate (k, T^{-1}) to the saturating pool can be regulated as a function of the
90 C saturation ratio (Hassink and Whitmore, 1997) (Fig. 1b). In both cases, when the saturation
91 ratio increases, ε and k effectively decrease because they are regulated multiplicatively by the
92 function $(1 - C_s/C_x)$ (Fig. 1). These two methods of implementing C saturation dynamics create
93 explicit couplings between C saturation and N mineralization dynamics in different ways, the
94 implications of which have not been explored.

95 The N mineralization in Eq. (1) applies to any transfer of C and N between pools. The
96 extent to which net N mineralization occurs as opposed to net N immobilization depends on the
97 magnitude of ε and the difference between r_{dec} and r_{rec} . The r of decomposing plant residue can
98 vary widely across residue types. The critical r (r_{cr}) below which decomposing residue will
99 cause positive net N mineralization can be solved using Eq. (1) when $N_{m-imm}=0$, as shown in Eq.
100 2.

$$r_{cr} = \frac{r_{rec}}{\varepsilon} \quad (2)$$

101 This equation shows that a decrease in ε will increase r_{cr} . For example, if the receiving pool is
102 saturated, the r_{cr} of decomposing substrates increases. The biological meaning of a decreasing ε
103 is that a smaller fraction of the products of microbial decomposition stabilize in organo-mineral
104 associations and thus remain available for further microbial decomposition. The r_{cr} in Eq. (2) is
105 for a single transfer and not for the sum of all transfers in a whole soil. A single transfer may
106 immobilize N while a simultaneous transfer among other pools in the soil may result in net N
107 mineralization at the whole soil level.

108 Although the coupling of C and N cycles in soils is largely mediated by microbial
109 biomass, the microbial pool has been given little consideration in saturation models. In only one
110 case is the microbial pool explicitly represented in the model structure (Hassink and Whitmore,

111 1997). This is in contrast to the body of contemporary C models in whole, where 60% of models
112 include one or more microbial pools (Manzoni and Porporato, 2009). In other C saturation
113 models, the microbial pool is either not included (Stewart et al., 2007) or is implicitly included
114 when parameterizing ϵ (Kemanian et al., 2011). In the latter model, ϵ lumps in one step what is a
115 cascade of C transfers among pools mediated by microbial turnover. While this approach may
116 produce reasonable results for net C exchange in monthly or yearly time frames, when these ϵ are
117 used for short time steps they may obscure the N cycling during microbial turnover.

118 A feature that implicitly links non-saturation and saturation C models is the role of soil
119 clay concentration (f_{clay}) in mediating ϵ , and hence N mineralization. In C saturation models, f_{clay}
120 is used to calculate the maximum size of the saturating pool (Hassink and Whitmore, 1997;
121 Kemanian et al., 2011), thus the C saturation ratio is a function of f_{clay} . Models that use the C
122 saturation ratio to regulate ϵ thus connect f_{clay} to ϵ . Non-saturating C cycling models have long
123 used f_{clay} to directly regulate ϵ (Parton et al., 1987; Jenkinson, 1990; Verberne et al., 1990) in a
124 way that leads to lower N mineralization rates and a lower r_{cr} in clay-rich soils. This method
125 originated from observations that soils with high f_{clay} stabilize a greater proportion of C inputs.
126 For example, Jenkinson (1990) and Parton et al. (1987) used relationships derived from Sørensen
127 (1975) and Sørensen (1981). However, Hassink (1996) found that the C saturation ratio of a soil
128 was a better predictor of C retention than f_{clay} , suggesting that C saturation may be a more
129 fundamental mechanism to integrate the effect of soil texture in a coupled C and N model.
130 Despite the commonalities in how f_{clay} controls N mineralization in both saturating and non-
131 saturating C models, the behavior of N mineralization in these two types of C models has never
132 been formally compared in the literature.

133 In summary, while N dynamics are mathematically linked to C cycling in models with
134 coupled elemental cycles, the implications of C saturation model structure for simulated N
135 mineralization dynamics have not been addressed nor have N mineralization dynamics in a C
136 saturation model been compared with that of non-saturation models. To advance the
137 understanding of these areas we propose a set of hypotheses about how the structure and
138 parameterization of different C models will affect the dynamics of a coupled N mineralization
139 model. First, the method used to implement C saturation in a model, either through regulation of
140 transfer efficiency (ϵ) or transfer rate (k), will affect N mineralization dynamics. Second, whether
141 or not C saturation models include an explicit microbial pool through which C and N must pass
142 will affect N mineralization dynamics. Finally, using ϵ to implement C saturation in a model
143 results in soil texture controls on N mineralization that are similar to those currently included in
144 widely used non-saturating C and N models. To test these hypotheses, we compared three
145 different C saturation models and one non-saturation model (Fig. 2). These model structures
146 were taken from the literature or developed for this investigation. Models varied in whether C
147 saturation regulated either ϵ or k and whether a microbial pool was included in the saturation
148 model. We coupled N to C cycling to obtain N mineralization and illustrate how the C model
149 structure affects the r_{cr} and the temporal dynamics of a simulated inorganic N pool during plant
150 residue decomposition.

151

152 **2. Methods**

153 *2.1. Structure of the Carbon Models*

154 We focused on three C saturation models with increasing complexity and one non-
155 saturation C model (Fig. 2). The first and simplest model in our study is a single-pool saturation

156 model, adapted from the models proposed by Kemanian et al. (2005, 2011) and Stewart et al.
157 (2007). The second model expands the single-pool saturation model by adding a microbial pool
158 (C_m). We termed this model the microbial saturation model to reflect the explicit inclusion of a
159 microbial pool through which C and N must pass. The third model is the abiotic saturation
160 model, whose structure was proposed by Hassink and Whitmore (1997). This model includes a
161 microbial pool (C_m), a labile unprotected pool (C_{un}), and a saturating pool of protected C (C_s).
162 We called this the abiotic saturation model because the saturating pool is directly linked to the
163 labile pool and any transfers are abiotic sorption and desorption. We compared these three C
164 saturation models to the Rothamsted C (RothC) model (Jenkinson, 1990), which is based on first
165 order kinetics and results in a linear relationship between C input and steady-state C level.

166 Because the main purpose of this study is to compare how the structure of C models
167 affects N mineralization, rather than C storage, we forced the turnover rate parameters so that
168 each model would return similar steady-state C stocks at a given level of fresh C inputs. We used
169 turnover rates from RothC as defaults and the resulting steady state soil C as a reference for other
170 models. A detailed description of each model is provided in the following sections. For
171 reference, model structures are diagrammed in Fig. 2, parameters are specified in Table 1, and
172 the differential equation for each pool is in Table 2.

173 **2.1.1. Single-pool Saturation Model**

174 In the single-pool saturation model, decomposed C from the pool of residue inputs (C_r) is
175 transferred directly to C_s . The ϵ from C_r to C_s is regulated by an efficiency factor (ϵ_x) and the
176 saturation ratio (C_s/C_x). We calculate C_x as a function of f_{clay} using the formula developed by
177 Hassink and Whitmore (1997). In this model, ϵ_x represents a humification coefficient (*sensu*
178 Hénin and Dupuis, 1945), or the slope that would be obtained by regressing dC_s/dt against C

179 inputs. This coefficient is an effective efficiency that lumps the C use efficiency of the microbes
180 feeding on residues and on microbial biomass (predation), detritus and exudates. We used $\epsilon_x =$
181 $0.18 \text{ g C g}^{-1} \text{ C}$. This value is in the upper range reported by Huggins et al. (1998), and would
182 correspond to three cycles of microbial feeding with a C use efficiency of $0.56 \text{ g C g}^{-1} \text{ C}$ (i.e.,
183 0.56^3). This C use efficiency agrees well with a representative upper value in soils reported in
184 Fig. 6 of Manzoni et al. (2012). Both C_r and C_s decay with first order kinetics according to the
185 rate constants in Table 1. Decomposed C that is not transferred to C_s is respired as CO_2 . The
186 turnover rate of soil C (k_s) in this model is taken from RothC. The residue C pool turnover rate
187 (k_r) in all three saturation models is taken as the weighted average of the turnover rates for
188 decomposable (k_{dpm}) and resistant (k_{rpm}) plant material input pools in RothC (i.e.,
189 $0.59k_{dpm}+0.41k_{rpm}$).

190

191 **2.1.2. Microbial Saturation Model**

192 In the microbial saturation model, C decomposed from C_r and C_s is transferred to C_m
193 while C decomposed from C_m is transferred to C_s . The ϵ from decomposing pools to receiving
194 pools is calculated as the square root of the ϵ used in the single-pool saturation model. Thus, C
195 that is stepping from C_r to C_m and from C_m to C_s is retained with an overall efficiency similar to
196 the single-pool model. Decomposed C that is not transferred to a receiving pool is respired as
197 CO_2 . The three pools C_r , C_m , and C_s decay with first order kinetics. The turnover rate of the
198 microbial pool (k_m) in this model is taken from RothC while k_s is derived to maintain a steady
199 state C_s level that is equivalent to the single-pool saturation model. The derivation for k_s is
200 provided in Appendix A.

201

202 **2.1.3. Abiotic Saturation Model**

203 The abiotic saturation model is adapted from the structure proposed by Hassink and
204 Whitmore (1997). Decomposed C from C_r and C_{un} is transferred to C_m with a fixed ε
205 representing microbial C use efficiency. Carbon in C_{un} is also transferred to C_s , a protected pool,
206 simulating the abiotic sorption of organic C to mineral surfaces. The transfer rate from C_{un} to C_s
207 (k_{un-s}) is controlled by a maximum rate that is regulated by the size of C_s relative to its maximum
208 capacity (C_x), with the latter being calculated as a function of f_{clay} using the original linear
209 regression developed by Hassink and Whitmore. Transfer of C from C_s to C_{un} , representing the
210 desorption of organic C from the mineral phase, occurs at the rate k_s . Because the sorption-
211 desorption process is abiotic, the ε between C_{un} and C_s is 1 (no CO_2 is respired in the transfer).
212 The turnover rates k_r and k_m are consistent with the other saturation models. We set the default
213 value for the decay rate k_{un} at 0.01 d^{-1} while the decay rates k_{un-s} and k_s were derived such that
214 steady state C_s level would be equivalent to the single-pool saturation model (see Appendix A for
215 the derivation).

216

217 **2.1.4. Rothamsted C Model**

218 In the RothC model (Jenkinson, 1990), C pools include decomposable (C_{dpm}) and
219 resistant (C_{rpm}) fractions of plant material inputs, and microbial (C_m) and stabilized (C_s) pools of
220 soil C. Each pool decays with its own first-order rate constant. Decomposed C from each pool
221 is transferred to the receiving pools with an efficiency (ε) that is determined by f_{clay} . This
222 efficiency varies from a low of 0.15 at 0.01 clay concentration to a plateau of approximately 0.24
223 at 0.45 clay concentration. The fraction of decomposed C that is not transferred to a receiving

224 pool $(1 - \epsilon)$ is respired as CO_2 . Of the total C decomposed from all pools and not lost as CO_2 ,
225 54% is transferred to C_s and 46% is transferred to C_m .

226

227 2.2. Modeling N mineralization

228 We coupled a simple N mineralization-immobilization model to each of the four C
229 models using the convention described in Eq. (1). The coupling of C and N for each model
230 structure is diagrammed in Fig. 2. In this N mineralization model, N decomposes from the donor
231 pool in proportion to C decomposition based on the r_{dec} . A portion of the decomposed C is
232 transferred to a receiving pool based on ϵ , while the remaining C is respired as CO_2 .
233 Decomposed organic N is transferred to the receiving pool in proportion to the C received by the
234 pool based on the r_{rec} . Nitrogen mineralization (or immobilization) is calculated as the difference
235 between the N decomposed and the N assimilated by the receiving pool. Nitrogen mineralized as
236 a result of C decomposition is added to an inorganic N (N_i) pool. When $N_{\text{m-imm}}$ is negative,
237 immobilization occurs and N is removed from the N_i pool. If the pool size of N_i is insufficient to
238 meet the immobilization demand, C decomposition is limited by N availability, as we assume
239 that ϵ will not change. Under such circumstances, we calculate the reduced C decomposition by
240 rearranging Eq. (1) and assuming that $N_i + N_{\text{m-imm}} = 0$:

241

$$C_{\text{dec}} = \frac{N_i}{\frac{\epsilon}{r_{\text{rec}}} - \frac{1}{r_{\text{dec}}}} \quad (16)$$

242

243 We use a fixed r of 10 for the microbial and soil organic matter pools while the r of the input
244 residues was a variable parameter input to the model.

245 To maintain simplicity of our N model, we do not include N transformations such as
246 nitrification or N losses such as leaching and plant uptake. Thus, in time series modeling
247 exercises, the N_i pool represents the cumulative sum of net N mineralization and immobilization.
248 Due to the simplification of our N model, we do not include N cycling feedbacks on C cycling,
249 which are known to exist in nature and are sometimes included in more sophisticated models
250 (e.g. Schimel and Weintraub, 2003; Eliasson and Ågren, 2011)

251

252 2.3. Modeling Exercises

253 To study and illustrate the differences in C and N cycling among the four models and the
254 implications of the C model structure on N mineralization we did the following: (i) derived the
255 analytical solutions to the steady-state size of each C pool as a function of C input level for all
256 models; (ii) calculated the r_{cr} for a range of f_{clay} and saturation ratios; and (iii) simulated the
257 temporal dynamics of N mineralization at a daily time-step following a one-time residue
258 addition.

259 In the daily time-step residue addition simulation, a 5 Mg C ha^{-1} mass of plant residues
260 with a r of 60 added to the soil on day 1 was allowed to decompose for 365 days. Nitrogen
261 mineralization and/or immobilization resulting from residue and soil organic matter
262 decomposition was added to or removed from the N_i pool. The simulation was conducted for
263 0.05 clay concentration and 0.25 clay concentration soils. Soil organic C pool sizes in each
264 model were initialized to steady-state levels for an annual plant residue addition level of 5 Mg C
265 ha^{-1} (equations in Table 3). The N_i pool was initialized to a size of $0.05 \text{ Mg N ha}^{-1}$ to prevent N
266 limitation of decomposition during the modeling exercise. Simulations were conducted in
267 Microsoft Excel using the Visual Basic for Applications programming language.

268

269 3. Results

270 3.1. Characteristics and Behavior of the C Models

271 As expected, steady-state levels of C pools in each model responded to increasing C
272 inputs in either a saturating or linear manner based on the parameterization of each model
273 structure (Table 3 and Fig. 3). The C_s pool saturates in all three saturation models and C_m
274 saturates in the microbial saturation model. In the single-pool saturation and microbial saturation
275 models, this results because the C transfer efficiency (ϵ) to C_s and C_m is regulated by the C
276 saturation ratio. As C saturation increases, more C is respired as CO_2 in the transfer and less is
277 retained by the receiving pool. The C_s pool saturates in the abiotic saturation model because k_{un-s}
278 is regulated by the C saturation ratio. As C saturation increases, less C is transferred from C_{un} to
279 C_s . In the abiotic saturation model, C_m and C_{un} are non-saturating and respond linearly to
280 increasing C inputs, as do all the pools in RothC. The linear response is because the ϵ to these
281 pools is a fixed value. Increasing f_{clay} from 0.05 to 0.25 led to increased C storage in the C_s
282 pools of all saturation models and RothC, and the C_m pools of the microbial saturation model and
283 RothC (Fig. 3). In the abiotic saturation model, C_m and C_{un} levels were unaffected by f_{clay} .

284 When C input levels and soil clay concentration were low, only small differences in total
285 C storage were predicted by each model, as calculated by summing the mass of all C pools (Fig.
286 3c and 3d). However, at higher C input levels and soil clay concentration, large divergences
287 between the saturation models and RothC occurred owing to the asymptotic characteristic of
288 saturation models. Even though the abiotic saturation model contained the non-saturating pools
289 C_{un} and C_m , the overall response of total C storage to increasing C inputs was similar to that of a
290 pure saturation model. This is because of the relatively small size of the C_{un} and C_m pools

291 compared to C_s when C inputs are within the range typical of most ecosystems ($<15 \text{ Mg C ha}^{-1} \text{ y}^{-1}$).
292 ¹).

293

294 3.2. Nitrogen Mineralization Dynamics

295 The method used to implement C saturation in a model, by regulating either transfer
296 efficiency (ϵ) or transfer rate (k), affected N mineralization dynamics. When C saturation is
297 implemented by regulating ϵ , as in the single-pool saturation and microbial saturation models,
298 the saturation ratio affects the r_{cr} of decomposing plant residues (Table 4, Fig. 4a). In these
299 models, r_{cr} increases as the saturation ratio increases. On the other hand, when C saturation is
300 implemented by regulating k , as in the abiotic saturation model, r_{cr} is independent of the
301 saturation ratio (Table 4, Fig. 4a).

302 The explicit inclusion of a microbial pool in the C saturation models also affected N
303 mineralization dynamics. When a microbial pool was not explicitly included, as in the single-
304 pool saturation model, r_{cr} ranged from 55 to nearly 1,000 over the saturation ratio gradient (Fig.
305 4a). In the microbial saturation and abiotic saturation models, where C and N flow through a
306 microbial pool, r_{cr} was lower and had a narrower range over the saturation ratio gradient. In the
307 microbial saturation model, r_{cr} ranged from 25 to 200 over the saturation ratio gradient while the
308 abiotic saturation model had a fixed r_{cr} of 40 (Figure 4a). The inclusion of a microbial pool also
309 affected the temporal dynamics of N mineralization during simulated residue decomposition. In
310 the microbial saturation and abiotic saturation models, decomposition of plant residue with $r=60$
311 led to an initial period of net N immobilization, whereas the single-pool saturation model
312 predicted immediate net N mineralization (Fig. 5).

313 Using ϵ to implement C saturation in the single-pool saturation and microbial saturation
314 models led to soil texture controls on N mineralization that were similar to RothC, a widely used
315 non-saturating model. In these three models, r_{cr} decreased as clay concentration increased (Fig.
316 4b). The r_{cr} in RothC decreased from 59 at a clay concentration of 0.05 to 41 at a clay
317 concentration of 0.80. Across the same clay concentration gradient, r_{cr} in the single-pool
318 saturation model decreased from 86 to 66 and r_{cr} in the microbial saturation model decreased
319 from 29 to 26.

320

321 **4. Discussion**

322 A significant result from our work is that despite similar predictions of C storage across
323 the saturation models, dynamics of N mineralization diverged widely due to the structure of each
324 model. We revealed two important considerations for how C saturation models can be linked to
325 N mineralization dynamics. First, the influence of C saturation on N mineralization dynamics
326 depends on whether C saturation is modeled as a process regulating transfer efficiencies or a
327 process regulating transfer rates. Second, a single-pool C saturation model that may predict
328 long-term C storage well can misrepresent short-term N mineralization if N cycling is simply
329 linked to the long cadence of C cycling. For example, the single-pool C saturation model
330 predicted N mineralization from high r ratio litter inputs ($r > 60$) which normally result in N
331 immobilization (Manzoni et al., 2008; Sinsabaugh et al. 2013). This mismatch between C and N
332 cycling can be greatly improved by simply adding an intermediate pool of microbial biomass
333 through which C and N must pass; an addition that does not affect long term C cycling. Finally,
334 we demonstrated that soil texture controls on N mineralization can be similar between saturation
335 and non-saturation models. These findings have important implications about how the structure

336 of C saturation models affect N mineralization and offer new hypotheses about the links between
337 C saturation and N mineralization processes that should be tested with further research, as
338 described in the following sections.

339 **4.1. Regulating ϵ vs. k to implement C saturation affects N mineralization dynamics**

340 The influence of C saturation on N mineralization dynamics depends on whether C
341 saturation is modeled as a process regulating ϵ or k . In the single-pool and microbial saturation
342 models, the C saturation ratio is used to regulate ϵ , coupling C saturation and N mineralization
343 processes based on Eq. (1). In the abiotic saturation model, where the saturation ratio does not
344 regulate ϵ but rather k , C saturation does not affect N mineralization dynamics. These
345 differences in how the models simulate C saturation present contrasting hypotheses of how C
346 saturation could affect N mineralization dynamics.

347 If C saturation does affect N mineralization, there may be important implications for
348 ecosystem management. For example, increasing C inputs to an ecosystem to promote C
349 sequestration, or large disposals of manure in the soil, would move the soil closer to C saturation,
350 causing more N mineralization from the inputs and potentially increased N losses. Management
351 practices that redistribute SOC concentrations in a soil profile and mix layers with higher
352 saturation ratio (e.g. top layer in no-till systems) with layers of lower saturation, would result in
353 altered N mineralization patterns from crop residues.

354 A limited number of studies addressed these potential implications. Castellano et al.
355 (2012) presented a conceptual model linking C and N saturation theories which was supported by
356 evidence that increasing levels of C saturation reduced the transfer of $\text{NH}_4\text{-N}$ to mineral
357 associated organic matter and increased potential net nitrification. Similarly, McLauchlan
358 (2006) found that net N mineralization decreased as clay concentration increased in soils

359 aggrading C following agricultural abandonment. The findings of both of these studies are
360 consistent with the behavior of a C saturation model where the C saturation ratio regulates ϵ . In
361 such a model, increasing C saturation would reduce ϵ , resulting in less N immobilization (as in
362 Castellano et al., 2012) or greater N mineralization (as in McLauchlan, 2006).

363 **4.2. Inclusion of a microbial pool in C saturation models affects N mineralization** 364 **dynamics**

365 In order to obtain reasonable predictions of N mineralization from decomposing
366 plant residues, it was necessary to include an explicit microbial pool in the C saturation model.
367 In the single-pool saturation model, an explicit microbial pool is not included, rather an effective
368 C transfer efficiency between C_r and C_s lumps approximately three cycles of microbial predation
369 into one step. This approach has been used to accurately predict C storage over decadal time
370 scales (Kemanian and Stöckle, 2010) and a single-pool model offers the advantages of
371 parsimony (Stewart et al., 2007) and simplicity of calibration requirements (Kemanian and
372 Stöckle, 2010). However, when coupled to a model of N mineralization, the single-pool
373 saturation model yielded a r_{cr} that ranged from 55 to over 555 as the C saturation ratio rose
374 above 0.9 (Fig. 4a). This range of r_{cr} is above the range that has been observed across a variety
375 of ecosystem and substrate types except for woody residue substrates (Manzoni et al., 2008).

376 The steepness of the rise in r_{cr} as C saturation ratio increases in the single-pool model
377 could be tempered by exponentiating the C saturation ratio. For example, Kemanian et al. (2011)
378 raised the C saturation ratio to the sixth power. While this method may maintain r_{cr} at more
379 reasonable levels across a broader range of C saturation ratios, it only shifts the sharp rise in r_{cr}
380 to a higher saturation ratio and accentuates the steepness of the rise when it does occur.

381 In the single-pool model, the steep rise in r_{cr} as C saturation increases is unrealistic. A
382 simple modification, adding an intermediate pool representative of microbial biomass, greatly
383 improved the dynamics of N mineralization in the microbial saturation model. In this model, r_{cr}
384 ranged from 23 to over 74 as the C saturation ratio rose above 0.9 (Fig. 4a). A similar range of
385 r_{cr} values was observed in non-woody plant residues by Manzoni et al. (2010), though the range
386 was mostly explained by N concentration of the residues rather than C saturation of the soil.
387 Within C saturation ratios that would occur under a more realistic C input level ($\sim 5 \text{ Mg C ha}^{-1} \text{ y}^{-1}$),
388 the r_{cr} in the microbial saturation model ranged narrowly from 26 to 29 across a range of clay
389 concentrations (Fig. 4b). The abiotic saturation model predicted an r_{cr} of 40 based on a fixed
390 microbial growth efficiency (ϵ) of 0.25. The r_{cr} predicted by the two C saturation models with
391 explicit microbial pools fall closely in line with traditional estimates of r_{cr} that have been
392 developed for relatively N rich residues (Sinsabaugh et al., 2013).

393 Compared to a single pool saturation model, the addition of a microbial pool to a C
394 saturation model allows representing the short-term dynamics of N storage and turnover in
395 microbial biomass. This improvement is achieved while preserving estimates of C storage and at
396 the cost of only one additional parameter to the model. This improvement results in a model
397 structure that can be applied to a broader set of ecological processes including both C and N
398 cycling at short and long time scales.

399 **4.3. Soil texture controls on N mineralization can be similar between saturation and** 400 **non-saturation models**

401 Soil texture has direct and indirect regulating effects on ϵ in RothC, the single-pool
402 saturation and microbial saturation models, resulting in similar soil texture controls on N
403 mineralization among the saturation and non-saturation models. RothC uses f_{clay} to directly

404 regulate ε while the single-pool saturation and microbial saturation models use f_{clay} to regulate
405 C_x , thus affecting ε (Table 1). In all three of these models, r_{cr} decreases with increasing clay
406 concentration when the pool size for C_s is maintained constant (Fig. 4b). This occurs because a
407 greater fraction of C and N are transferred to stabilized pools in clay rich soils rather than being
408 mineralized. Early studies that demonstrated soil texture controls on N mineralization under a
409 paradigm of non-saturation C models (Ladd et al., 1981; Van Veen et al., 1985; Schimel, 1986)
410 are consistent with the behavior of C saturation models that use ε to implement saturation.
411 Therefore, C saturation theory may provide a mechanism to explain the effects of soil texture on
412 C and N cycling.

413 **4.4 Relevance to ecosystem processes and future research**

414 Although the currently limited data on the links between C saturation and N
415 mineralization dynamics seem to support a coupling of these processes (Castellano et al., 2012),
416 it does not permit assessing with certainty the practical significance of such a relationship. For
417 instance, at reasonable C input rates, the change in r_{cr} due to the effects of a clay gradient on the
418 C saturation ratio is rather minor in the microbial saturation model (e.g., 26 to 29 as in Fig. 4b).
419 The effect of C saturation on r_{cr} becomes much more pronounced as the saturation ratio increases
420 above 0.5 (Fig. 4a). This level of saturation requires high C inputs per unit of soil mass under
421 the current parameterization of our model, but can be achieved in the top layer of undisturbed
422 no-till agricultural soils or pasture lands (Mazzilli et al., 2014) or in low clay concentration soils
423 (Castellano et al., 2012).

424 Given the limited but encouraging data supporting the conceptual and quantitative link
425 between C saturation and N mineralization, we believe that further empirical research should be
426 pursued to test the hypothesis that C saturation is a mechanism that controls N mineralization. In

427 testing this hypothesis, it will be particularly important to design studies that utilize C saturation
428 gradients across similar soil textures, as one can argue that it is difficult to separate saturation
429 from clay concentration effects in the experiments reported in the literature (Ladd et al., 1981;
430 Van Veen et al., 1985; Schimel, 1986; McLauchlan, 2006; Castellano et al., 2012). A more
431 specific hypothesis generated by our work is that as C saturation ratio increases so does the r_{cr} of
432 decomposing plant residues. If this hypothesis is correct, further studies should evaluate its
433 practical implications for managing C and N in natural and managed ecosystems. For example, a
434 hypothesis for an applied field experiment might be that N mineralization dynamics are altered
435 by C saturation patterns occurring in soil profiles with stratified soil organic matter, such as those
436 in no-till agricultural systems. We also suggest conducting additional studies to verify and
437 improve our estimation of the maximum soil C storage capacity (C_x), as the quantitative
438 relationship between C saturation and N mineralization is sensitive to this value and our current
439 method of estimation is based on the results of only one study (Hassink and Whitmore, 1997).

440 Recent advances in the understanding of C cycling, including C saturation theory, need to
441 be incorporated into a new generation of ecosystem models (Schmidt et al., 2011) as exemplified
442 by Kemanian et al.(2011). Along with C saturation, others are active in incorporating microbial
443 priming effects (Wutzler and Reichstein, 2008; Perveen et al., 2014) and controls on microbial C
444 use efficiency (Allison et al., 2010; Wetterstedt and Ågren, 2011) into biogeochemical models.
445 Perveen et al. (2014) demonstrated that N cycling was affected by increased fresh C inputs from
446 elevated CO₂ in a priming effect model. Interestingly, the definition for microbial priming
447 proposed by Wutzler and Reichstein (2008), where “decomposition of one soil C pool is
448 influenced by the dynamics of another soil C pool,” also pertains to the structure of some C
449 saturation models we tested in this study. Controlling microbial C use efficiency based on

450 temperature has proven to be an important model feature that improves the representation of
451 temperature effects on C cycling (Allison et al., 2010; Wetterstedt and Ågren, 2011). Given the
452 sensitivity of N mineralization to C use efficiency that we observed in our study, temperature
453 controls on C use efficiency in a model are also likely to affect a coupled N cycle. A next step in
454 the development of new ecosystem models will be to test how models behave when several new
455 C cycling processes are implemented simultaneously.

456 **5. Conclusions**

457 We demonstrated that different C saturation model structures can produce similar predictions of
458 C storage, but that predictions of N mineralization can diverge widely. Inclusion of a microbial
459 pool in the microbial saturation model led to more reasonable predictions of N mineralization
460 compared to the single-pool saturation model. We also demonstrated that the link between C
461 saturation and N mineralization depends on whether C saturation is modeled as a process
462 regulating transfer efficiencies or transfer rates among pools in the model. In a C saturation
463 model in which the saturation ratio regulates the transfer efficiency, the N mineralization
464 dynamics across a soil texture gradient are similar to that of the non-saturating RothC model.
465 These findings lead to new hypotheses about the relationship between C saturation and N
466 mineralization that can be tested empirically, and offer a clear pathway to represent C saturation
467 and N mineralization dynamics.

468 **Acknowledgements**

469 We thank the two anonymous referees and handling editor Sébastien Fontaine for constructive
470 comments that improved the quality of this article. This work was supported by United States
471 Department of Agriculture AFRI Grant GEOW-2013-02824 and Cornell Grant #52110-9601
472 (Sungrant subcontract, United States Department of Transportation).

474 **References**

- 475 Allison, S. D., Wallenstein, M. D. and Bradford, M. A.: Soil-carbon response to warming
476 dependent on microbial physiology, *Nat. Geosci.*, 3(5), 336–340, 2010.
- 477 Baldock, J. . and Skjemstad, J. .: Role of the soil matrix and minerals in protecting natural
478 organic materials against biological attack, *Org. Geochem.*, 31(7-8), 697–710, 2000.
- 479 Castellano, M., Kaye, J., Lin, H., and Schmidt, J.: Linking Carbon Saturation Concepts to
480 Nitrogen Saturation and Retention, *Ecosystems*, 15, 175-187, 2012.
- 481 Eliasson, P. E. and Ågren, G. I.: Feedback from soil inorganic nitrogen on soil organic matter
482 mineralisation and growth in a boreal forest ecosystem, *Plant Soil*, 338(1-2), 193–203, 2010.
- 483 Gulde, S., Chung, H., Amelung, W., Chang, C. and Six, J.: Soil Carbon Saturation Controls
484 Labile and Stable Carbon Pool Dynamics, *Soil Sci. Soc. Am. J.*, 72(3), 605, 2008.
- 485 Hassink, J.: Preservation of Plant Residues in Soils Differing in Unsaturated Protective Capacity,
486 *Soil Sci. Soc. Am. J.*, 60, 487, 1996.
- 487 Hassink, J.: The capacity of soils to preserve organic C and N by their association with clay and
488 silt particles, *Plant Soil*, 191(1), 77–87, 1997.
- 489 Hassink, J., and Whitmore, A. P.: A Model of the Physical Protection of Organic Matter in Soils,
490 *Soil Sci. Soc. Am. J.*, 61, 131-139, 1997.
- 491 Heitkamp, F., Wendland, M., Offenberger, K. and Gerold, G.: Implications of input estimation,
492 residue quality and carbon saturation on the predictive power of the Rothamsted Carbon
493 Model, *Geoderma*, 170, 168–175, 2012.
- 494 Hénin, S., and Dupuis, M.: Essai de bilan de la matière organique du sol, *Ann. Agron.*, 15, 17-29,
495 1945.
- 496 Huggins, D. R., Clapp, C. E., Allmaras, R. R., Lamb, J. A., and Laysee, M. F.: Carbon dynamics
497 in corn-soybean sequences as estimated from natural Carbon-13 abundance, *Soil Sci. Soc.*
498 *Am. J.*, 62, 195-203, 1998.
- 499 Jenkinson, D. S.: The Turnover of Organic-Carbon and Nitrogen in Soil, *Philos. T. Roy. Soc. B*,
500 329, 361-368, 1990.
- 501 Kemanian, A. R., Manoranjan, V. S., Huggins, D. R., and Stöckle, C. O.: Assessing the
502 usefulness of simple mathematical models to describe soil carbon dynamics, 3rd USDA
503 Symposium on Greenhouse Gases & Carbon Sequestration in Agriculture and Forestry,
504 Baltimore, Maryland, March 21-24, 2005, 2005.
- 505 Kemanian, A. R., and Stöckle, C. O.: C-Farm: A simple model to evaluate the carbon balance of
506 soil profiles, *Eur. J. Agron.*, 32, 22-29, 2010.
- 507 Kemanian, A. R., Julich, S., Manoranjan, V. S., and Arnold, J. R.: Integrating soil carbon cycling
508 with that of nitrogen and phosphorus in the watershed model SWAT: Theory and model
509 testing, *Ecol. Model.*, 222, 1913-1921, 2011.
- 510 Ladd, J. N., Oades, J. M., and Amato, M.: Microbial biomass formed from ¹⁴C, ¹⁵N-labelled plant
511 material decomposing in soils in the field, *Soil Biol. Biochem.*, 13, 119-126, 1981.
- 512 Manzoni, S., Jackson, R. B., Trofymow, J. A., and Porporato, A.: The global stoichiometry of
513 litter nitrogen mineralization, *Science*, 321, 684-686, 2008.
- 514 Manzoni, S., and Porporato, A.: Soil carbon and nitrogen mineralization: Theory and models
515 across scales, *Soil Biol. Biochem.*, 41, 1355-1379, 2009.
- 516 Manzoni, S., Trofymow, J. A., Jackson, R. B., and Porporato, A.: Stoichiometric controls on
517 carbon, nitrogen, and phosphorus dynamics in decomposing litter, *Ecol. Monogr.*, 80, 89-
518 106, 2010.

519 Manzoni, S., Taylor, P., Richter, A., Porporato, A., and Ågren, G. I.: Environmental and
520 stoichiometric controls on microbial carbon-use efficiency in soils, *New Phytol.*, 196, 79-91,
521 2012.

522 Mazzilli, S., Kemanian, A., Ernst, O., Jackson, R., Piñeiro, G.: Priming of soil organic carbon
523 decomposition induced by corn compared to soybean crops, Accepted in *Soil Biol.*
524 *Biochem.*: 2014.

525 McLaughlan, K. K.: Effects of soil texture on soil carbon and nitrogen dynamics after cessation
526 of agriculture, *Geoderma*, 136, 289-299, 2006.

527 Parton, W. J., Schimel, D. S., Cole, C. V., and Ojima, D. S.: Analysis of factors controlling soil
528 organic matter levels in Great Plains grasslands, *Soil Sci. Soc. Am. J.*, 51, 1173-1179, 1987.

529 Perveen, N., Barot, S., Alvarez, G., Klumpp, K., Martin, R., Rapaport, A., Herfurth, D., Louault,
530 F. and Fontaine, S.: Priming effect and microbial diversity in ecosystem functioning and
531 response to global change: a modeling approach using the SYMPHONY model., *Glob.*
532 *Chang. Biol.*, 20(4), 1174–90, 2014.

533 Schimel, D. S.: Carbon and nitrogen turnover in adjacent grassland and cropland ecosystems,
534 *Biogeochemistry*, 2, 345-357, 1986.

535 Schimel, J. P. and Weintraub, M. N.: The implications of exoenzyme activity on microbial
536 carbon and nitrogen limitation in soil: a theoretical model, *Soil Biol. Biochem.*, 35(4), 549–
537 563, 2003.

538 Schmidt, M. W. I., Torn, M. S., Abiven, S., Dittmar, T., Guggenberger, G., Janssens, I. a, Kleber,
539 M., Kögel-Knabner, I., Lehmann, J., Manning, D. a C., Nannipieri, P., Rasse, D. P.,
540 Weiner, S. and Trumbore, S. E.: Persistence of soil organic matter as an ecosystem
541 property., *Nature*, 478(7367), 49–56, 2011.

542 Sinsabaugh, R. L., Manzoni, S., Moorhead, D. L., and Richter, A.: Carbon use efficiency of
543 microbial communities: stoichiometry, methodology and modelling, *Ecol. Lett.*, 16, 930-939,
544 2013.

545 Six, J., Conant, R. T., Paul, E. A. and Paustian, K.: Stabilization mechanisms of soil organic
546 matter: Implications for C-saturation of soils, *Plant Soil*, 241(2), 155–176, 2002.

547 Sørensen, L. H.: The influence of clay on the rate of decay of amino acid metabolites synthesized
548 in soils during decomposition of cellulose, *Soil Biol. Biochem.*, 7, 171-177, 1975.

549 Sørensen, L. H.: Carbon-nitrogen relationships during the humification of cellulose in soils
550 containing different amounts of clay, *Soil Biol. Biochem.*, 13, 313-321, 1981.

551 Stewart, C. E., Paustian, K., Conant, R. T., Plante, A. F., and Six, J.: Soil carbon saturation:
552 concept, evidence and evaluation, *Biogeochemistry*, 86, 19-31, 2007.

553 Stewart, C. E., Plante, A. F., Paustian, K., Conant, R. T., and Six, J.: Soil carbon saturation:
554 Linking concept and measurable carbon pools, *Soil Sci. Soc. Am. J.*, 72, 379-392, 2008.

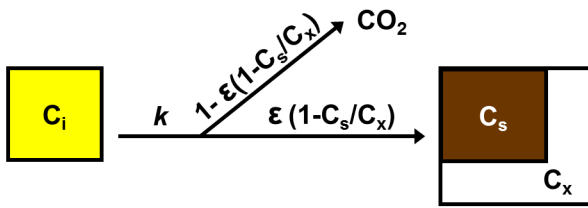
555 Stewart, C. E., Follett, R. F., Wallace, J., and Pruessner, E. G.: Impact of Biosolids and Tillage
556 on Soil Organic Matter Fractions: Implications of Carbon Saturation for Conservation
557 Management in the Virginia Coastal Plain, *Soil Sci. Soc. Am. J.*, 76, 1257-1267, 2012.

558 Van Veen, J. A., Ladd, J. N., and Amato, M.: Turnover of Carbon and Nitrogen through the
559 Microbial Biomass in a Sandy Loam and a Clay Soil Incubated with [¹⁴C(U)]Glucose and
560 [¹⁵N] (NH₄)₂SO₄ under Different Moisture Regimes, *Soil Biol. Biochem.*, 17, 747-756, 1985.

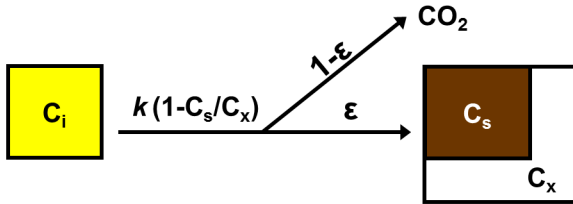
561 Verberne, E. L. J., Hassink, J., Dewilligen, P., Groot, J. J. R., and Van Veen, J. A.: Modeling
562 Organic-Matter Dynamics in Different Soils, *Neth. J. Agr. Sci.*, 38, 221-238, 1990.

- 563 Wetterstedt, J. Å. M. and Ågren, G. I.: Quality or decomposer efficiency – which is most
564 important in the temperature response of litter decomposition? A modelling study using the
565 GLUE methodology, *Biogeosciences*, 8(2), 477–487, 2011.
- 566 Wutzler, T. and Reichstein, M.: Colimitation of decomposition by substrate and decomposers- a
567 comparison of model formulations, *Biogeosciences*, 5, 749–759, 2008.

A. Saturation ratio regulates ϵ

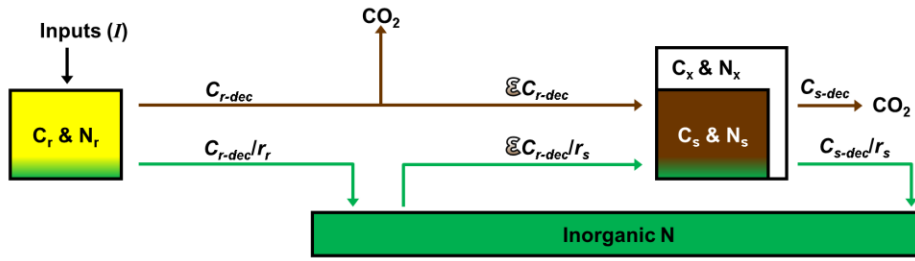


B. Saturation ratio regulates k

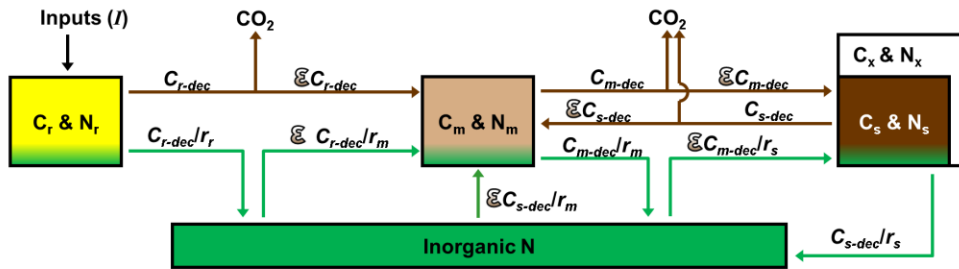


568
 569 Figure 1. Conceptual models illustrating two different methods of implementing C saturation
 570 dynamics. In both models, the C saturation ratio of the saturating pool is defined by the ratio of
 571 the current pool size (C_s) to a theoretical maximum pool size (C_x), or C_s/C_x . In model A, the C
 572 saturation ratio regulates the C transfer efficiency (ϵ) between the donor pool (C_i) and C_s . As the
 573 C saturation ratio increases, less of the C decomposed from C_i is transferred to C_s and more is
 574 respired as CO_2 . In model B, the C saturation ratio regulates the decomposition rate (k) of C_i ,
 575 such that the rate decreases as the C saturation ratio increases. The C transfer efficiency is not
 576 affected by the C saturation ratio in model B.
 577

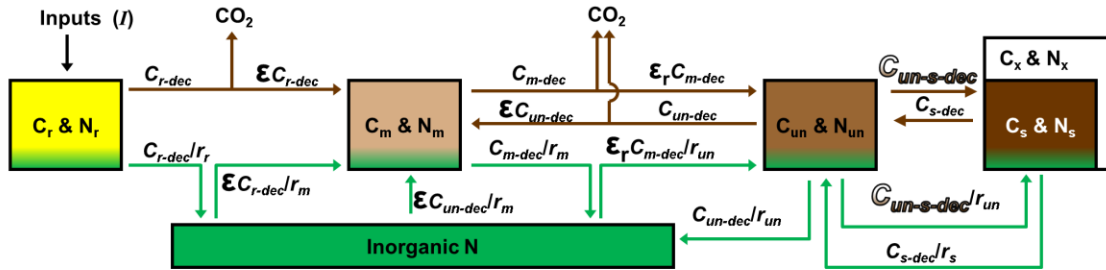
A. Single-pool Saturation



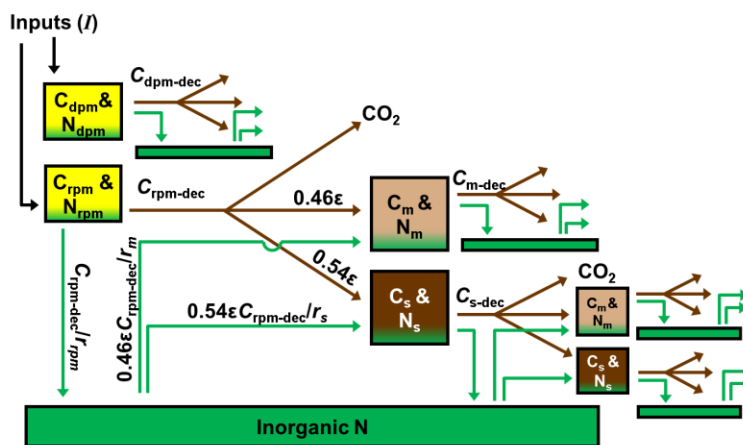
B. Microbial Saturation



C. Abiotic Saturation

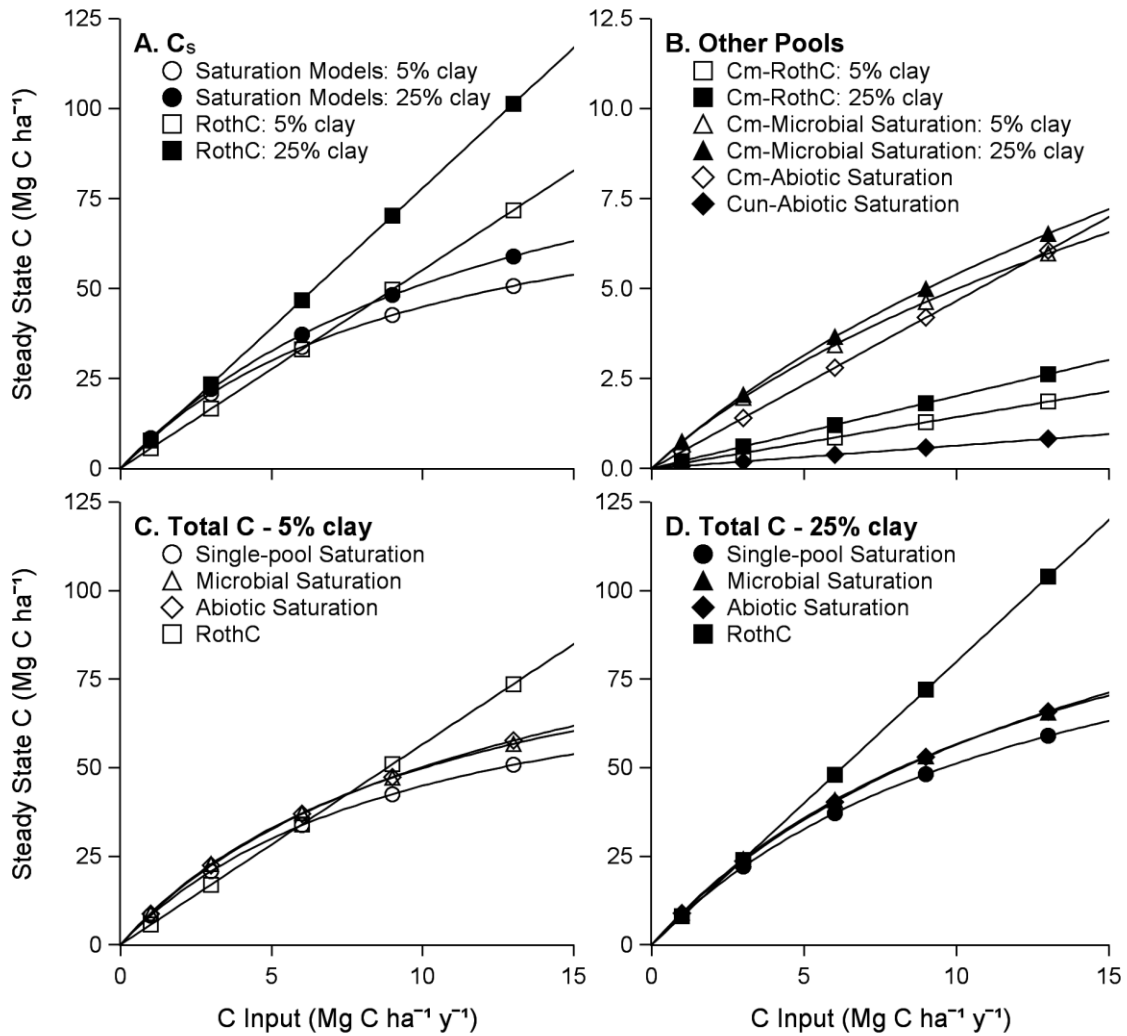


D. RothC



580 **Figure 2.** Diagrams of the pools and fluxes in the four models used in this study. Carbon and N
581 pools are indicated together in boxes. Carbon fluxes are indicated by brown arrows and N fluxes
582 by green arrows. Pools are abbreviated as follows: C_r, C_{dpm}, C_{rpm} and N_r, N_{dpm}, N_{rpm} are plant
583 residues; C_m and N_m are microbial biomass; C_{un} and N_{un} are un-protected soil organic matter; C_s
584 and N_s are protected or stabilized soil organic matter; C_x and N_x are the maximum or saturating
585 capacity for C and N storage. The inorganic N pool is represented by a green box. Carbon
586 decomposition from each pool and the pool stoichiometry (C:N ratio) are represented by the
587 symbols C_{j-dec} and r_j , respectively, where j specifies the pool. Pools decompose with first order
588 kinetics based on rates listed in Table 1. The symbol ϵ is the C transfer efficiency to the
589 receiving pool, the value of which is specified by Table 1 for each model. Symbols illustrated
590 with a brown gradient fill pattern are regulated by the C saturation ratio (C_s/C_x).

591



592

593 **Figure 3.** The relationship between C input level and the steady-state C level of various

594 pools in each model for soils with contrasting clay concentration. (A) The C_s pool of

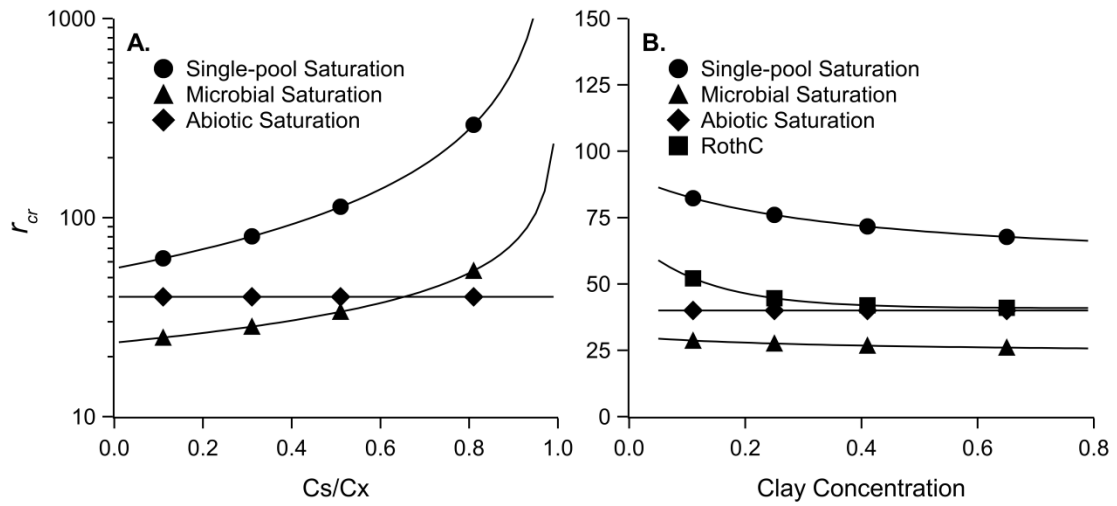
595 each model in soils with 0.05 and 0.25 clay concentration. (B) Other C pools in each

596 model in soils with 0.05 and 0.25 clay concentration (note: the pools in the abiotic

597 saturation model are not sensitive to clay concentration). (C, D) The total C pool size in

598 soils with 0.05 clay concentration (C) and 0.25 clay concentration (D).

599



600

601 **Figure 4.** The critical C:N ratio (r_{cr}) as a function of carbon saturation ratio (A) and clay

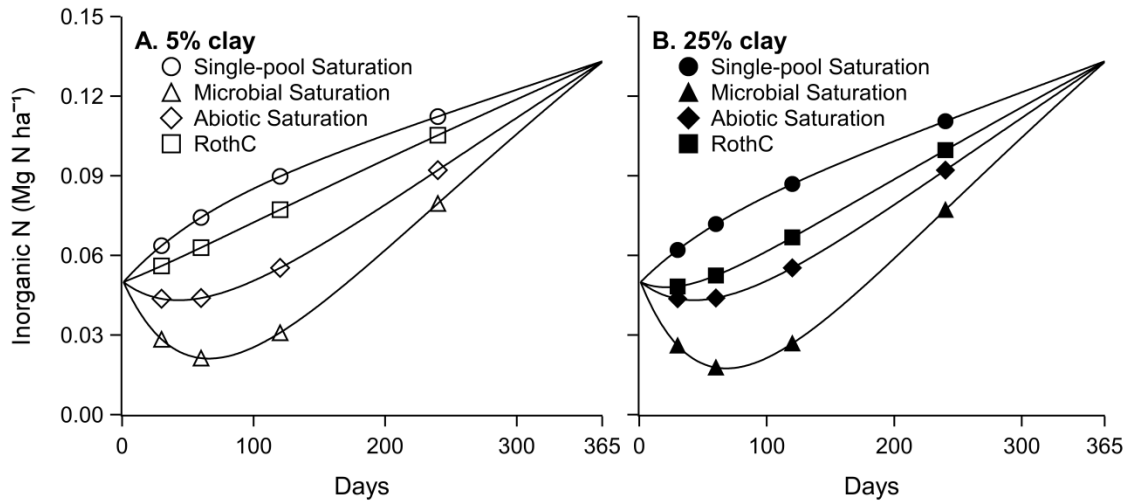
602 concentration (B). In (B), the pool size for C_s was maintained constant at 32 Mg C ha⁻¹,

603 thus the clay gradient creates a C saturation gradient. For reference, a pool size of 32 Mg

604 C ha⁻¹ would result from an annual C input level of ~5 Mg C ha⁻¹ y⁻¹.

605

606



607

608

609 Figure 5. The inorganic N pool during decomposition of a 5 Mg C ha⁻¹ residue addition

610 with a *r* of 60 in a soil with 0.05 clay concentration (A) and 0.25 clay concentration (B).

611 Soil C pool sizes for each model structure were initialized to the steady state levels that

612 would occur from annual residue additions of 5 Mg C ha⁻¹. Residue and soil C pools

613 decomposed at the optimum rates listed in Table 1.

614 Table 1. The parameter values used in each model.

Parameter	Description	Units	Single-pool Saturation	Microbial Saturation	Abiotic Saturation	RothC
C_x^a	Maximum capacity of C_s	$g\ C\ kg^{-1}\ soil$	$21.1 + 37.5f_{clay}$	$21.1 + 37.5f_{clay}$	$21.1 + 37.5f_{clay}$	
ϵ_x	Humification coefficient	$g\ C\ g^{-1}\ C$	0.18	0.18	0.18	
ϵ	Carbon transfer efficiency	$g\ C\ g^{-1}\ C$	$\epsilon_x(1 - C_s/C_x)$	$\sqrt{\epsilon_x(1 - C_s/C_x)}$	0.25	$\frac{1}{4.09 + 2.67e^{-7.86f_{clay}}}$
ϵ_r	Carbon recycling efficiency	$g\ C\ g^{-1}\ C$			0.75	
k_r	Residue decomposition rate	d^{-1}	0.0165	0.0165	0.0165	
k_{dpm}	Labile residue decomposition rate	d^{-1}				0.0274
k_{rpm}	Recalcitrant residue decomposition rate	d^{-1}				8.2×10^{-4}
k_s	C_s decomposition rate	d^{-1}	5.48×10^{-5}	$\frac{5.48 \times 10^{-5}}{(1 - \epsilon^2)}$	$\frac{5.48 \times 10^{-5}}{k_{un}(1 - \epsilon \epsilon_r)}$	5.48×10^{-5}
k_m	C_m decomposition rate	d^{-1}		1.81×10^{-3}	$\frac{1.81 \times 10^{-3}}{1.81 \times 10^{-3}}$	1.81×10^{-3}
k_{un-s}	Transfer rate from C_{un} to C_s	d^{-1}			$\frac{\epsilon_x(1 - C_s/C_x)}{\epsilon \epsilon_r}$	
k_{un}	C_{un} decomposition rate	d^{-1}			0.01	

^a C_x as calculated by Hassink and Whitmore (1997). For use in the modeling exercises, we converted C_x to units of $Mg\ C\ ha^{-1}$ by assuming a soil bulk density of $1.3\ Mg\ m^{-3}$ and a soil depth of 0.3 m.

Table 2. Differential equations for carbon pools in each model.

Single-pool saturation model

$$dC_r/dt = I^a - k_r C_r \quad (3)$$

$$dC_s/dt = \varepsilon k_r C_r - k_s C_s \quad (4)$$

Microbial saturation model

$$dC_r/dt = I - k_r C_r \quad (5)$$

$$dC_m/dt = \varepsilon k_r C_r + \varepsilon k_s C_s - k_m C_m \quad (6)$$

$$dC_s/dt = \varepsilon k_m C_m - k_s C_s \quad (7)$$

Abiotic saturation model

$$dC_r/dt = I - k_r C_r \quad (8)$$

$$dC_m/dt = \varepsilon k_r C_r + \varepsilon k_{un} C_{un} - k_m C_m \quad (9)$$

$$dC_{un}/dt = \varepsilon_r k_m C_m + k_s C_s - k_{un} C_{un} - k_{un-s} C_{un} \quad (10)$$

$$dC_s/dt = k_{un-s} C_{un} - k_s C_s \quad (11)$$

RothC

$$dC_{dpm}/dt = 0.59I - k_{dpm} C_{dpm} \quad (12)$$

$$dC_{rpm}/dt = 0.41I - k_{rpm} C_{rpm} \quad (13)$$

$$dC_s/dt = 0.54 \varepsilon (k_{dpm} C_{dpm} + k_{rpm} C_{rpm} + k_m C_m + k_s C_s) - k_s C_s \quad (14)$$

$$dC_m/dt = 0.46 \varepsilon (k_{dpm} C_{dpm} + k_{rpm} C_{rpm} + k_m C_m + k_s C_s) - k_m C_m \quad (15)$$

^a I = Plant residue C inputs

615

616

Table 3. Analytical solutions to the steady-state level of the SOC pools in each model. Carbon input rate (I) and turnover rates k_s , k_m , and k_{un} must have same time units.

All saturation models

$$C_s = \frac{\varepsilon_x I}{k_s^a + \varepsilon_x C_r / C_x} \quad (17)$$

Microbial saturation model

$$C_m = \frac{\sqrt{\varepsilon_x(1 - C_s/C_x)} I}{k_m(1 - \varepsilon_x(1 - C_s/C_x))} \quad (18)$$

Abiotic saturation model

$$C_m = \frac{\varepsilon I}{k_m(1 - \varepsilon \varepsilon_r)} \quad (19)$$

$$C_{un} = \frac{\varepsilon \varepsilon_r I}{k_{un}(1 - \varepsilon \varepsilon_r)} \quad (20)$$

RothC

$$C_s = \frac{0.54\varepsilon I}{k_s(1 - \varepsilon)} \quad (21)$$

$$C_m = \frac{0.46\varepsilon I}{k_m(1 - \varepsilon)} \quad (22)$$

^aThe k_s parameter value from the single-pool saturation model.

Table 4. The analytical solution to r_{cr} in each model.

Single-pool saturation

$$r_{cr} = \frac{r_s}{\varepsilon_x(1 - C_s/C_x)} \quad (23)$$

Microbial saturation

$$r_{cr} = \frac{r_m}{\sqrt{\varepsilon_x(1 - C_s/C_x)}} \quad (24)$$

Abiotic saturation

$$r_{cr} = \frac{r_m}{0.25} \quad (25)$$

RothC

$$r_{cr} = (0.54r_s + 0.46r_m) (4.0 + 2.67e^{-7.86f_{clay}}) \quad (26)$$

620

621

622 **Appendix A**

623 Deriving the parameter k_s for the microbial saturation model that would force steady-state
624 C_s levels to be equivalent to the single-pool saturation model required reformulating Eq.
625 (7) to solve dC_s/dt with respect to C_r . This is achieved by solving steady-state Eq. (6) for
626 $k_m C_m$ and substituting this for $k_m C_m$ in Eq. (7). The result is Eq. (A1):

$$dC_s/dt = \varepsilon^2 k_r C_r - (1 - \varepsilon^2) k_s C_s \quad (\text{A1})$$

627

628 Eq. (A1) and Eq. (4) can be equated and the turnover rate for C_s in model B solved:

$$k_s = \frac{5.48 \times 10^{-5}}{(1 - \varepsilon^2)} \quad (\text{A2})$$

629

630 To derive parameters for the abiotic saturation model that would force steady-state C_s
631 levels to be equivalent to steady-state C_s levels in the single-pool saturation model we
632 reformulated Eq. (11) to solve dC_s/dt with respect to C_r . This required rearrangements of
633 Eq. (10) and Eq. (9) along with several substitutions. First, steady-state Eq. (9) was
634 solved for $k_m C_m$ and substituted into Eq. (10), which was then solved for C_{un} . The
635 resulting equation for C_{un} was substituted into Eq. (11), yielding:

$$dC_s/dt = \varepsilon_r \varepsilon k_{un-s} k_r C_r - k_{un} (1 - \varepsilon_r \varepsilon) k_s C_s \quad (\text{A3})$$

636

637 Eq. (A3) and Eq. (4) can be equated and the decay rates k_{un-s} and k_s solved:

638

$$k_{un-s} = \frac{\varepsilon_x (1 - C_s/C_x)}{\varepsilon \varepsilon_r} \quad (\text{A4})$$

$$k_s = \frac{5.48 \times 10^{-5}}{k_{\text{un}}(1 - \varepsilon \varepsilon_r)} \quad (\text{A5})$$